University of Reading

Revisiting trends in wetness and dryness in the presence of internal climate variability and water limitations over land

Article

Published Version

www.reading.ac.uk/centaur

Revisiting trends in wetness and dryness in the presence of internal climate variability and water limitations over land

Sanjiv Kumar[1], Richard P. Allan[2], Francis Zwiers[1], David M. Lawrence[3], and Paul A. Dirmeyer[4]

[1]Pacific Climate Impacts Consortium, University of Victoria, Victoria, British Columbia, Canada, [2]Department of Meteorology, University of Reading, Reading, UK, [3]National Center for Atmospheric Research, Boulder, Colorado, USA, [4]Center for Ocean-Land-Atmosphere Studies, George Mason University, Fairfax, Virginia, USA

Abstract A theoretically expected consequence of the intensification of the hydrological cycle under global warming is that on average, wet regions get wetter and dry regions get drier (WWDD). Recent studies, however, have found significant discrepancies between the expected pattern of change and observed changes over land. We assess the WWDD theory in four climate models. We find that the reported discrepancy can be traced to two main issues: (1) unforced internal climate variability strongly affects local wetness and dryness trends and can obscure underlying agreement with WWDD, and (2) dry land regions are not constrained to become drier by enhanced moisture divergence since evaporation cannot exceed precipitation over multiannual time scales. Over land, where the available water does not limit evaporation, a "wet gets wetter" signal predominates. On seasonal time scales, where evaporation can exceed precipitation, trends in wet season becoming wetter and dry season becoming drier are also found.

1. Introduction

Movement of water vapor in the atmosphere is the fundamental quantity that results in the spatially variable hydroclimatic (precipitation minus evaporation, $P - E$) patterns, including wet conditions in convergence zones (e.g., deep tropics, monsoonal regions, and some middle- and high-latitude regions) and dry conditions in divergence zones (e.g., subtropical regions) [*Allan*, 2014; *Seager et al.*, 2010]. The atmospheric water vapor concentration increases with global warming following the Clausius-Clapeyron relationship [*Stull and Ahrens*, 2000]. Satellite data and ground-based observations show evidence of increased atmospheric water vapor concentration [*Allan*, 2014; *Chung et al.*, 2014; *Santer et al.*, 2007]. When more water-laden air parcels move through the atmosphere, they enhance $P - E$ in convergence zones and $E - P$ in divergence zones; a simplified description of the theory is known as wet gets wetter and dry gets drier (WWDD) [*Greve et al.*, 2014] as outlined by *Held and Soden* [2006].

The sensitivity of global precipitation change is much smaller (2%/K) than the sensitivity of water vapor concentration change (7%/K), and this is primarily because the atmosphere and surface cannot lose sufficient radiative energy to accommodate the additional latent heating within the radiative-convective balance [*Chadwick et al.*, 2013; *Held and Soden*, 2006; *O'gorman et al.*, 2012]. Reduced convective mass flux as part of diminishing atmospheric circulation strength is one way in which the atmosphere adjusts in reconciling the water vapor and precipitation changes [*Bony et al.*, 2013; *Vecchi and Soden*, 2007]. This reduces but does not negate the enhancement of $P - E$ patterns with global warming [*Allan*, 2012; *Chadwick et al.*, 2013].

The moisture-driven changes are modulated regionally by variations in atmospheric circulations. A weakening of the tropical circulation leads to opposite effects, i.e., wet gets drier and dry gets wetter (WDDW) [*Chadwick et al.*, 2013; *Chou et al.*, 2009; *Seager et al.*, 2010, 2014]. More locally, spatial movement of high rainfall regimes toward usually drier regions and vice versa will also lead to WDDW [*Allan*, 2014; *Chou et al.*, 2009] and these responses are also strongly influenced by internal climate variability [*Deser et al.*, 2010, 2012; *Gu and Adler*, 2013; *O'gorman et al.*, 2012]. Large-scale circulation changes, e.g., expansion of the Hadley cell, extend subtropical dry zones poleward [*Lu et al.*, 2007; *Scheff and Frierson*, 2012], and a poleward shift in storm tracks contributes to subtropical drying and poleward moistening [*Scheff and Frierson*, 2012; *Seager et al.*, 2010]. *Byrne and O'Gorman* [2015] found a drying tendency over land relating to spatial gradients in temperature changes, e.g., polar amplification and greater warming over land than

oceans. Hence, while the circulation changes produce dynamical changes in both convergence and divergence zones, the moisture-driven changes are an emerging signal of global warming [*Chou et al.*, 2013; *Liu and Allan*, 2013].

Recent studies have found significant discrepancies between the WWDD theory and observed changes over land. *Greve et al.* [2014] found that the WWDD theory holds over 10.8% of land areas and does not hold for 13.8% land areas, based on observations from 1948 to 2005, with the remainder of the land area not showing statistically significant changes. Hence, Greve et al. concluded that the WWDD theory can be *potentially misleading* over the land. However, contrasting results between theoretical understanding and observation-based findings can be reconciled by considering a number of factors: the nature and sensitivity of metrics [*Allan*, 2014], the definition of wet and dry regions and time averaging over wet and dry seasons [*Chou et al.*, 2013; *Liu and Allan*, 2013], and effects of internal variability and water limitations to evaporation over land (discussed here). Here we provide an important clarification that is necessary for increasing confidence in the underpinning physical principles of changes in the hydrological cycle.

2. Data and Method

We employed climate simulations for preindustrial, historical, and future climates from four Coupled Model Intercomparison Project Phase 5 (CMIP5) climate models (CanESM2, CCSM4, CNRM-CM5, and MPI-ESM-MR) that have long (~1000 years) preindustrial climate simulations available in the CMIP5 archive [*K. E. Taylor et al.*, 2012]. All available ensemble members are employed (supporting information Table S1). To avoid biases due to having more ensemble members from one climate model than another, we used a multimodel ensemble weighted average approach [*Jones et al.*, 2013]. Model data are regridded to a common $2.5° \times 2.5°$ resolution using an area average preserving method.

The dryness index (DI, equation (1)) metric is used to assess wetness and dryness trends

$$\mathrm{DI} = \frac{R_n}{\lambda \cdot P} \qquad (1)$$

where R_n is net radiation at the surface, λ is latent heat of vaporization, and P is precipitation, all of which are computed from 20 year climatological means [see also *Greve and Seneviratne*, 2015; *Roderick et al.*, 2015; *Roderick et al.*, 2014]. DI less than 1.0 represents energy-limited (wet) regions, and greater than 1.0 represents water-limited (dry) regions. We used a slightly adjusted threshold DI, based on preindustrial climate simulations (range: 1.25 to 1.5; supporting information Figure S1), so that all land area between 60°S and 90°N is equally divided between wet and dry regions. The adjusted threshold reduces model uncertainties and provides spatially consistent distributions of wet and dry regions across four climate models, e.g., the wet and dry contrast between the eastern and western United States (supporting information Figure S2). Results presented here are not sensitive to the adjusted threshold DI (supporting information Figures S3 and S7).

We also employ the precipitation minus evaporation ($P - E$) metrics on seasonal time scales, since the DI metric is relevant only over annual mean or longer time scales [*Zhang et al.*, 2008]. Trends in $P - E$ are computed for local (grid cell) wet and dry 3 month seasons corresponding to maximum and minimum $P - E$ in the seasonal cycle [*Kumar et al.*, 2014a]. To account for changes in seasonality under global warming, we determined wet and dry seasons for each nonoverlapping 20 year period from 1850 to 2100 (supporting information Figure S4).

We employed a "perfect model analysis" by comparing model-simulated changes against model-simulated internal variability [*Dirmeyer et al.*, 2013; *Holland et al.*, 2013; *Kumar et al.*, 2014b; *Tietsche et al.*, 2014]. We estimated the local (grid cell) variability of 20 year mean DI climatologies that is due to internal variations by calculating the variance of DI from nonoverlapping 20 year periods in preindustrial climate simulations. Changes in DI relative to the preindustrial mean in the historical or future climates (Representative Concentration Pathways (RCP)4.5 and RCP8.5) are deemed significant (<5% significance) if they are greater than 2 standard deviations in magnitude [*Arnell and Gosling*, 2013; *Kumar et al.*, 2014a]. We performed a similar analysis for the 20 year mean wet and dry seasons' $P - E$ and compared it with the preindustrial $P - E$ in the corresponding season.

3. Results

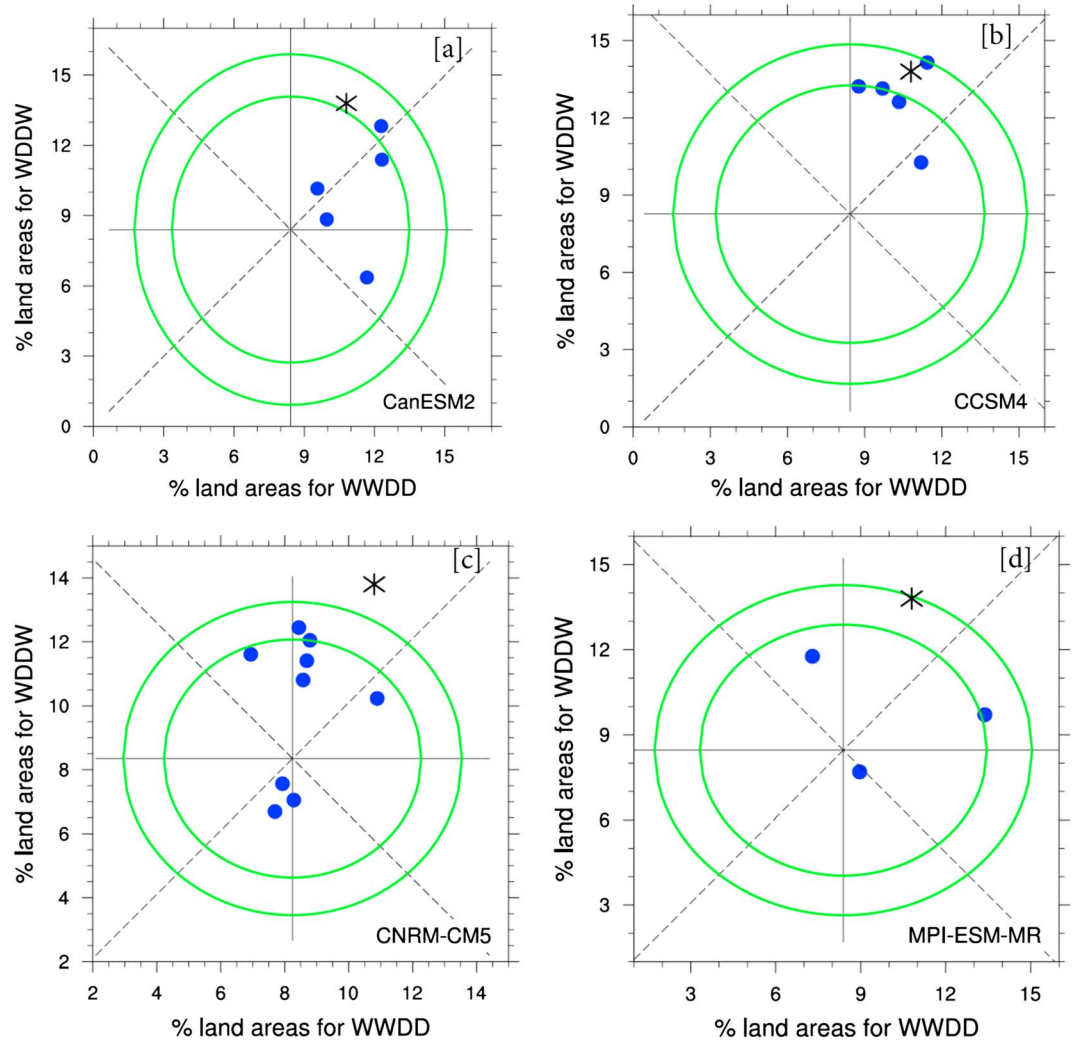### 3.1. Role of Internal Variability

Decadal to multidecadal climate variability strongly affects local/regional trends, e.g., the warming hole in the eastern United States, and precipitation recovery in western Sahel after a prolonged drought in the 1970s and 1980s [*Deser et al.*, 2012; *Dong and Sutton*, 2015; *Kumar et al.*, 2013b; *Meehl et al.*, 2015; *Villamayor and Mohino*, 2015]. To assess that, we sampled nonrepeating 60 year data segments from preindustrial climate simulations and studied trends in wetness and dryness as the differences between the last and first 20 years. The 60 year data length allows comparison to changes assessed from observational records of similar length [*Greve et al.*, 2014]. For example, 1000 year preindustrial climate simulation results in 50 nonoverlapping 20 year samples for the calculation of DI (DI_i, $i = 1, 2,\dots 50$) and 48 overlapping 60 year samples ($DI_{i+2} - DI_i$, $i = 1, 2,\dots 48$). Similarly calculated changes for historical periods are evaluated locally against control run trend variability for significance. Areas of significant changes are grouped under two categories: (1) WWDD and (2) WDDW.

Figure 1 shows two circles/ellipses representing 95% and 99% confidence regions for trends in wetness and dryness due internal climate variability in preindustrial climate simulations (see supporting information for details). Clearly, a large spread in wetness and dryness trends can be expected only due to internal climate variability over any 60 year period; the multimodel mean WWDD trends are found in $8.4 \pm 4.9\%$ of the land area and the same for WDDW trends (the uncertainty ranges are 95% confidence intervals). Trends in historical simulations of the period 1948 to 2005 are mostly within the uncertainty envelope of preindustrial simulations (Figure 1). The *Greve et al.* [2014] results, which are based on observations and show that more land area with significant DI trends falls within the WDDW realm than the WWDD realm, lie on the edges of the uncertainty envelopes; the null hypothesis of consistency with climate model-simulated internal variability would be rejected at the 5% significance level in three cases (CanESM2, CCSM4, and MPI-ESM-MR) and at the 1% significance level in the case of the fourth model (CNRM-CM5). Please also note that circles/ellipses provide a conservative estimate of internal variability because of (1) overlapping 60 year periods (supporting information Figure S5) and (2) uncertainty in climate models particularly related to decadal to multidecadal climate variability [*Chadwick et al.*, 2015; *Knutson et al.*, 2013; *Kumar et al.*, 2013b]. Analysis of large ensemble climate simulations [*Kay et al.*, 2015] also shows significant uncertainty due to internal climate variability in future projections (supporting information Figure S6).

3.2. Effects of Climate Change on Wetness and Dryness Trends in a Perfect Model Analysis

To study DI changes in historical and future climate simulations (RCP4.5 and RCP8.5), we identify significant DI changes relative to preindustrial mean DI for each nonoverlapping 20 year period between 1901 and 2100 (i.e., 1901–1920, 1921–1940,…, 2006–2025,…, 2081–2100). The resulting time series of DI changes under WWDD and WDDW categories, separately for land and oceans, is shown in Figure 2. The amount of area that exhibits significant change in DI increases with global warming, as expected, with the higher emission scenario (RCP8.5) exhibiting greater total percentage area with significant change than the medium emission scenario (RCP4.5). Over land, the changes fall into the WWDD and WDDW categories roughly equally throughout the historical and future periods [see also *Greve and Seneviratne*, 2015]. This is in stark contrast to the oceans where the WWDD theory operates strongly.

Figure 3 shows the spatial distribution of significant changes ($<5\%$ significance level) at the end of the 20th and the 21st centuries, both relative to preindustrial climate. The effect of climate change is evident with the lowest DI change areas seen by end of the 20th century and the highest fractional areas showing change in RCP8.5 projections. In global warming scenarios, drying of subtropical dry zones, particularly over the oceans, is evident (DD, Figures 3c and 3d). Drying of ocean refers to increase in DI or enhancement of $E - P$. Some dry land areas that become drier include ocean-continental boundary regions in the subtropical dry zones, e.g., Mediterranean, Mexico, and western Sahel. Wet gets wetter (WW) areas are found in the deep tropics convergence zone including central east Africa (Congo Basin), Pacific coast of northwestern South America, parts of Southeast Asia, and middle- to high-latitude regions in both hemispheres (around 60°S and 60°N, respectively). Dry areas becoming wetter (DW) include central Asia, central eastern Africa, eastern Sahel, and southern South America. Some wet areas of the tropical and subtropical oceans become drier (WD), and vice versa (DW), and these areas tend to lie between the boundary of atmospheric convergence (wet) and divergence (dry) zones. WD and DW trends in the boundary regions can be related to

Figure 1. Role of internal variability in wetness and dryness trends. The two circles/ellipses represent 95% and 99% confidence regions for wetness and dryness trends in the preindustrial climate simulations. Historical simulation corresponding to observation period (1948 to 2005) is shown in blue dots that represent each ensemble member. The result from Greve et al. is shown using an asterisk. Somewhat different sizes and shapes of uncertainty circles/ellipses are indicative of the climate model's uncertainties.

circulation-driven dynamical changes, e.g., dry advection from neighboring descending zones or a shift in convergence zones [*Chou et al.*, 2009; *Joetzjer et al.*, 2013]. Wet gets drier (WD) areas, as measured by DI, are found in the Arctic regions, possibly because of sea ice and snow cover loss, and the snow-albedo feedback leading to increased absorption of incident solar radiation, less energy needed for snow and sea ice melt, and more energy available for evaporation and thereby an increased DI [*Bony et al.*, 2006; *DelSole et al.*, 2014; *Zhang et al.*, 2015].

3.3. Explaining Uncertainties in Wetness and Dryness Trends Over Land

The fundamental premise of the WWDD theory is that more evaporated water from divergence zones will contribute to greater precipitation in convergence zones. But evaporation greater than precipitation is not possible over sustained time periods in dry land regions because of limited water availability, unlike the oceans which have unlimited water availability in both convergence and divergence zones. Hence, the main mechanism by which dry regions become drier (DD) is not relevant over land; therefore, it is hypothesized that the WWDD theory is applicable mainly in "wet" areas where evaporation is not limited by the available water but by the available energy, i.e., land regions where $DI < 1.0$.
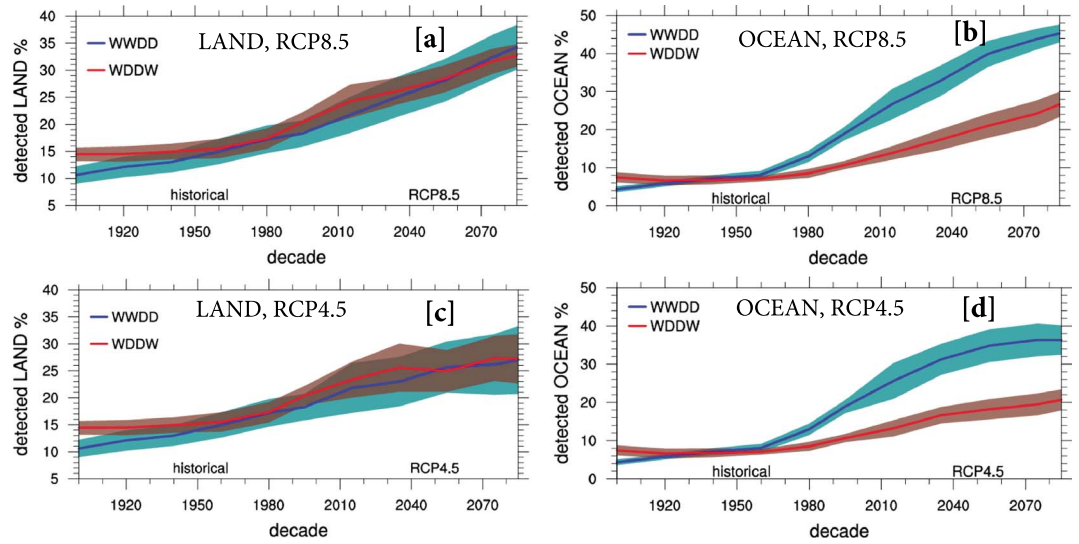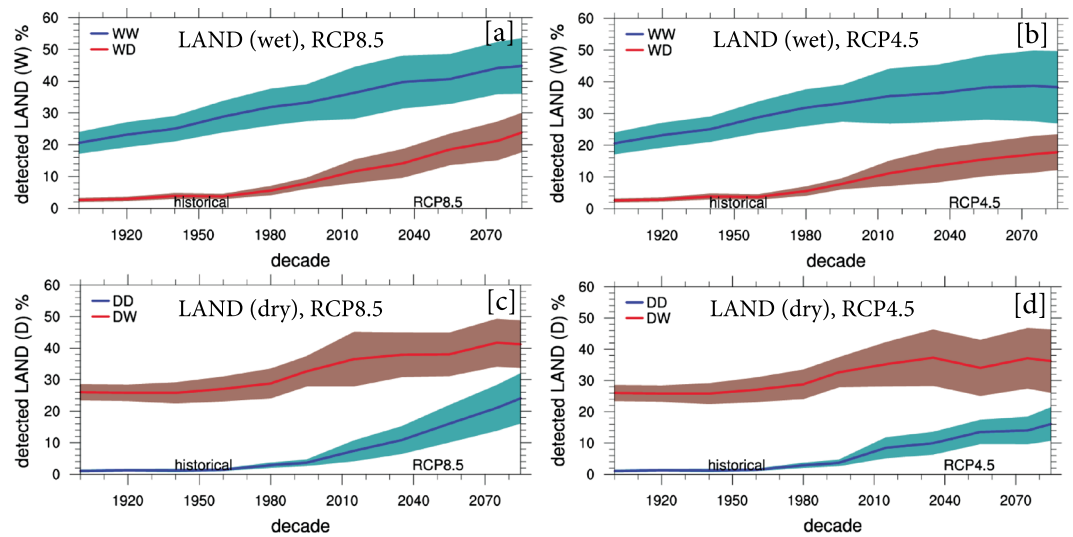
Figure 2. The multimodel mean wetness and dryness trends in historical, RCP4.5, and RCP8.5 climate simulations relative to preindustrial climate over (a and c) land and (b and d) oceans. Unit: percent areas in each category showing significant trends. Figures 2a and 2b show RCP8.5 and Figures 2c and 2d RCP4.5. Shaded bands represent 95% confidence interval estimates of the mean.

Figure 4 shows assessment of the WWDD theory in wet and dry land regions separately (see also supporting information Table S2). In wet regions, WW areas are more frequently encountered than WD areas, whereas in dry regions, more dry land areas get wetter (DW) than drier (DD). This makes sense because most dry areas receive precipitation of advective origin (large scale) [*Dirmeyer and Brubaker*, 2007], and, with higher average atmospheric water vapor content in a warmer climate, one would expect the resulting increases in moisture
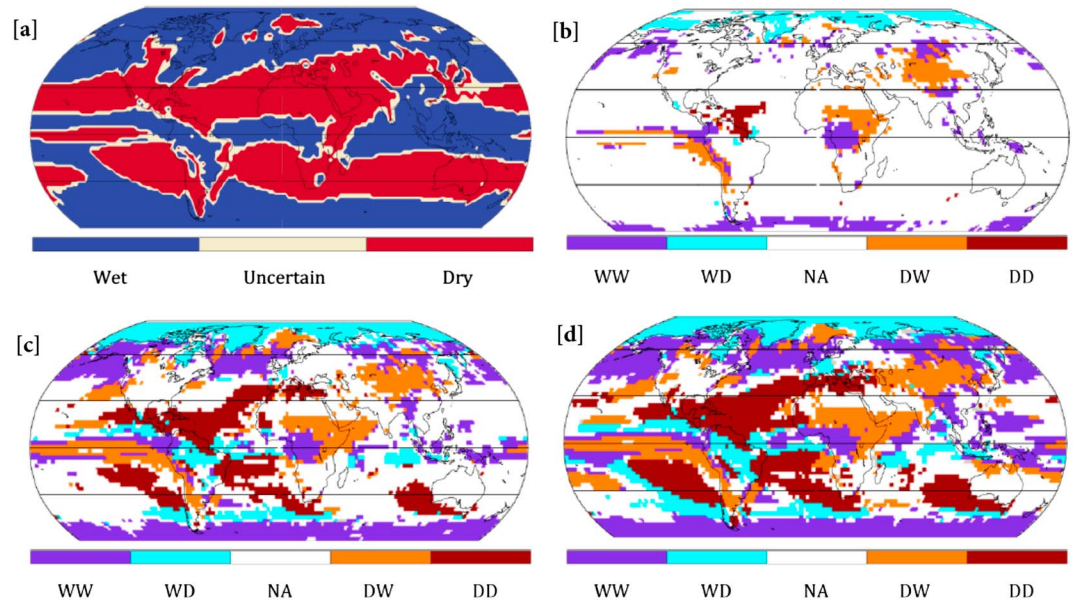
Figure 3. Spatial distribution of (a) wet and dry regions, (b) wetness and dryness trends at the end of the 20th century (1986 to 2005), (c) at the end of the 21st century (2081 to 2100) in RCP4.5 projections, and (d) the same for RCP8.5 projections. Wet and dry regions are defined based on majority rule (≥3 out of 4 models). Uncertain areas represent equal division between four models, i.e., two models dry and two models wet. Only statistically significant trends at or less than 5% significance level are shown. Trends are shown if 65% or more of ensemble members show a significant trend, in which case the majority direction of trend is shown in the figure: wet gets wetter (WW), wet gets drier (WD), dry gets wetter (DW), and dry gets drier (DD).

Figure 4. The multimodel mean wetness and dryness trends in historical, RCP4.5, and RCP8.5 climate simulations relative to preindustrial climate for (a and b) wet land regions defined as DI ≤ 1.0 (nominally) and for (c and d) dry land regions defined as DI > 1.0 (nominally). Unit: percent areas in each category showing significant trends. Shaded bands represent 95% confidence interval estimates of the mean.

advection leading to more precipitation in these areas. Nevertheless, a shift in precipitation patterns and local feedback processes can bring significant changes of both signs in dry regions [*Chadwick et al.*, 2015; *Guillod et al.*, 2015; *C. M. Taylor et al.*, 2012].

Figure 5 shows trends in $P - E$ in local wet and dry seasons (see also supporting information Table S2). In wet regions and wet seasons, higher WW trends occur 8 to 11 times more often than WD trends. Similarly, in dry regions and dry seasons, higher DD trends occur 4 to 5 times more often than DW trends. Please note that evaporation can exceed precipitation on seasonal time scales [e.g., *Sheffield et al.*, 2013]. In dry regions and wet seasons, significantly higher (4 to 5 times) DW trends than DD trends are also found. In wet regions and dry seasons, a generally higher (1.2 to 1.5 times) WD than WW trends are found, but these two trends are not significantly different. Overall, seasonal analysis supports the notion that wet season becomes wetter and dry season becomes drier [*Chou et al.*, 2013; *Kumar et al.*, 2014a].

4. Discussion and Conclusions

Comparing simulated historical changes (Figure 3b) with observed changes reported in *Greve et al.* [2014] reveals several differences such as wetting trends in the eastern U.S. and the western Sahel that are not seen in the majority of model simulations. Both of these regions are known to be substantially influenced by multidecadal climate variability that is either internally generated or radiatively forced or some combination of these two [*Dong and Sutton*, 2015; *Kumar et al.*, 2013b; *Meehl et al.*, 2015; *Villamayor and Mohino*, 2015]. Uncertainty in the observations, e.g., poor data coverage in Africa, South America, and Asia, may also be a factor [*Koster et al.*, 2011; *Kumar et al.*, 2013a]. Uncertainties in climate models, e.g., land-atmosphere coupling and feedback processes, can also be an issue [*Guillod et al.*, 2015; *Kumar et al.*, 2013c; *Pitman et al.*, 2009; *C. M. Taylor et al.*, 2012]. Nonetheless, we have minimized the effects of model uncertainties by using perfect model analysis [*Dirmeyer et al.*, 2013; *Holland et al.*, 2013; *Kumar et al.*, 2014b; *Tietsche et al.*, 2014].

The other source of uncertainty is using potential evaporation (PET) instead of net radiation in equation (1) that shifts the validity of the WWDD theory toward the drier branch (DD) rather than the wetter branch (WW), although it does not affect overall uncertainties over land (supporting information Figures S8 and S9) [see also *Greve and Seneviratne*, 2015]. Over land, the potential evaporation computed using Food and Agricultural Organization's Penman-Monteith method increases at a much faster rate (5–6%/°C of warming) than precipitation changes (2%/°C) [*Fu and Feng*, 2014; *Roderick et al.*, 2015; *Scheff and Frierson*, 2014]. Hence, the PET-based calculation favors drying. Since changes in net radiation are comparable to

Wet Season
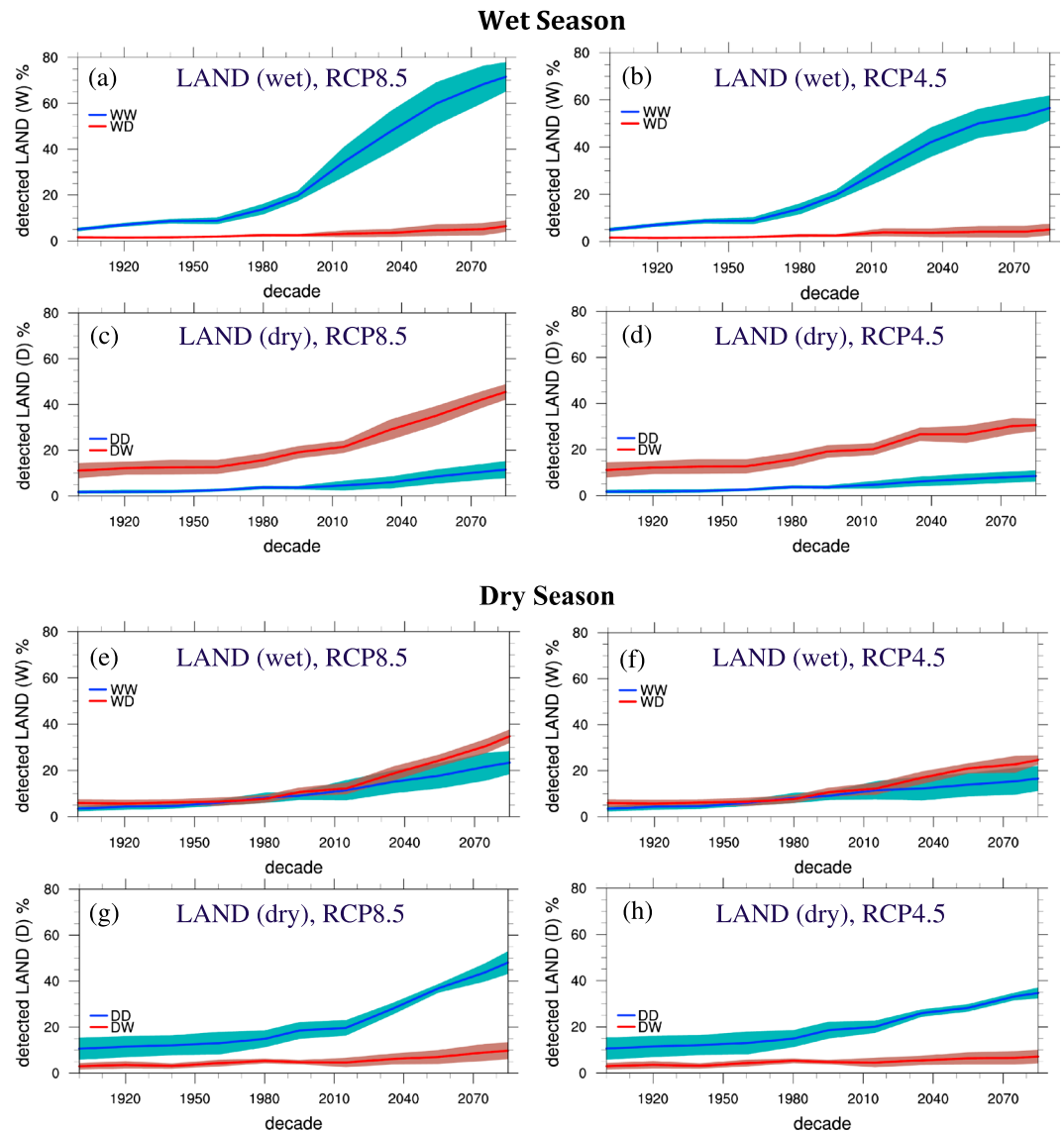
Dry Season

Figure 5. The multimodel mean wetness and dryness trends in (a–d) local wet seasons and (e–h) local dry seasons. Time series obtained using historical and RCP8.5 climate simulations are shown in Figures 5a, 5c, 5e, and 5g and using historical and RCP 4.5 climate simulations are shown in Figures 5b, 5d, 5f, and 5h. Unit: percent areas in each category showing significant trends. Shaded bands represent 95% confidence interval estimates of the mean.

precipitation and evaporation changes [*Roderick et al.*, 2015], the net radiation-based DI changes and $P - E$ changes are consistent (Figures 4 and 5). It is also worth noting uncertainties in PET estimate due to different methodologies, e.g., temperature-based Thornthwaite and physically based Penman-Monteith methods [*Sheffield et al.*, 2012].

Overall, we have provided several important clarifications. First, internal variability alone can obscure underlying agreement with the WWDD theory (Figure 1). Second, most of the uncertainties come from dry land regions (Figure 4), which are not constrained to become drier by enhanced moisture divergence since evaporation cannot exceed precipitation over multiannual time scales. Third, we provided evidence that supports the WWDD theory in wet land regions at annual time scales. On seasonal time scales, where evaporation can exceed precipitation, trends in wet season becoming wetter and dry season becoming drier are also found (Figure 5). Based on these four points, we conclude that the WWDD theory remains a useful framework for the interpretation of hydroclimatic change where seasonality is considered and provided that internal variability and water limitations to evaporation in dry land areas are taken into account.

Taking both wet and dry land together on multiannual time scales, we also acknowledge the alternative viewpoint that does not support the WWDD theory over land as documented in previous studies [*Greve and Seneviratne*, 2015; *Greve et al.*, 2014; *Roderick et al.*, 2014].

References

Allan, R. P. (2012), Regime dependent changes in global precipitation, *Clim. Dyn.*, *39*(3–4), 827–840, doi:10.1007/s00382-011-1134-x.

Allan, R. P. (2014), Climate change: Dichotomy of drought and deluge, *Nat. Geosci.*, *7*(10), 700–701, doi:10.1038/ngeo2243.

Arnell, N. W., and S. N. Gosling (2013), The impacts of climate change on river flow regimes at the global scale, *J. Hydrol.*, *486*, 351–364.

Bony, S., et al. (2006), How well do we understand and evaluate climate change feedback processes?, *J. Clim.*, *19*(15), 3445–3482.

Bony, S., G. Bellon, D. Klocke, S. Sherwood, S. Fermepin, and S. Denvil (2013), Robust direct effect of carbon dioxide on tropical circulation and regional precipitation, *Nat. Geosci.*, *6*(6), 447–451.

Byrne, M. P., and P. A. O'Gorman (2015), The response of precipitation minus evapotranspiration to climate warming: Why the "wet-get-wetter, dry-get-drier" scaling does not hold over land, *J. Clim.*, *28*, 8078–8092, doi:10.1175/JCLI-D-15-0369.1.

Chadwick, R., I. Boutle, and G. Martin (2013), Spatial patterns of precipitation change in CMIP5: Why the rich do not get richer in the tropics, *J. Clim.*, *26*(11), 3803–3822.

Chadwick, R., P. Good, G. Martin, and D. P. Rowell (2015), Large rainfall changes consistently projected over substantial areas of tropical land, *Nat. Clim. Change*, doi:10.1038/nclimate2805.

Chou, C., J. D. Neelin, C.-A. Chen, and J.-Y. Tu (2009), Evaluating the "rich-get-richer" mechanism in tropical precipitation change under global warming, *J. Clim.*, *22*(8), 1982–2005.

Chou, C., J. C. H. Chiang, C.-W. Lan, C.-H. Chung, Y.-C. Liao, and C.-J. Lee (2013), Increase in the range between wet and dry season precipitation, *Nat. Geosci.*, *6*(4), 263–267.

Chung, E. S., B. Soden, B. J. Sohn, and L. Shi (2014), Upper-tropospheric moistening in response to anthropogenic warming, *Proc. Natl. Acad. Sci. U.S.A.*, *111*(32), 11,636–11,641.

DelSole, T., X. Yan, P. A. Dirmeyer, M. Fennessy, and E. Altshuler (2014), Changes in seasonal predictability due to global warming, *J. Clim.*, *27*(1), 300–311.

Deser, C., A. Phillips, V. Bourdette, and H. Teng (2010), Uncertainty in climate change projections: The role of internal variability, *Clim. Dyn.*, *38*(3–4), 527–546.

Deser, C., R. Knutti, S. Solomon, and A. S. Phillips (2012), Communication of the role of natural variability in future North American climate, *Nat. Clim. Change*, *2*(11), 775–779.

Dirmeyer, P. A., and K. L. Brubaker (2007), Characterization of the global hydrologic cycle from a back-trajectory analysis of atmospheric water vapor, *J. Hydrometeorol.*, *8*(1), 20–37.

Dirmeyer, P. A., S. Kumar, M. J. Fennessy, E. L. Altshuler, T. DelSole, Z. C. Guo, B. A. Cash, and D. Straus (2013), Model estimates of land-driven predictability in a changing climate from CCSM4, *J. Clim.*, *26*(21), 8495–8512.

Dong, B., and R. Sutton (2015), Dominant role of greenhouse-gas forcing in the recovery of Sahel rainfall, *Nat. Clim. Change*, *5*(8), 757–760.

Fu, Q., and S. Feng (2014), Responses of terrestrial aridity to global warming, *J. Geophys. Res. Atmos.*, *119*, 7863–7875, doi:10.1002/2014JD021608.

Greve, P., and S. I. Seneviratne (2015), Assessment of future changes in water availability and aridity, *Geophys. Res. Lett.*, *42*, 5493–5499, doi:10.1002/2015GL064127.

Greve, P., B. Orlowsky, B. Mueller, J. Sheffield, M. Reichstein, and S. I. Seneviratne (2014), Global assessment of trends in wetting and drying over land, *Nat. Geosci.*, *7*(10), 716–721.

Gu, G. J., and R. F. Adler (2013), Interdecadal variability/long-term changes in global precipitation patterns during the past three decades: Global warming and/or Pacific decadal variability?, *Clim. Dyn.*, *40*(11–12), 3009–3022.

Guillod, B. P., B. Orlowsky, D. G. Miralles, A. J. Teuling, and S. I. Seneviratne (2015), Reconciling spatial and temporal soil moisture effects on afternoon rainfall, *Nat. Commun.*, *6*, 6443, doi:10.1038/ncomms7443.

Held, I. M., and B. J. Soden (2006), Robust responses of the hydrological cycle to global warming, *J. Clim.*, *19*(21), 5686–5699.

Holland, M. M., E. Blanchard-Wrigglesworth, J. Kay, and S. Vavrus (2013), Initial-value predictability of Antarctic sea ice in the Community Climate System Model 3, *Geophys. Res. Lett.*, *40*, 2121–2124, doi:10.1002/grl.50410.

Joetzjer, E., H. Douville, C. Delire, and P. Ciais (2013), Present-day and future Amazonian precipitation in global climate models: CMIP5 versus CMIP3, *Clim. Dyn.*, *41*(11–12), 2921–2936.

Jones, G. S., P. A. Stott, and N. Christidis (2013), Attribution of observed historical near-surface temperature variations to anthropogenic and natural causes using CMIP5 simulations, *J. Geophys. Res. Atmos.*, *118*, 4001–4024, doi:10.1002/jgrd.50239.

Kay, J. E., et al. (2015), The Community Earth System Model (CESM) large ensemble project: A community resource for studying climate change in the presence of internal climate variability, *Bull. Am. Meteorol. Soc.*, *96*, 1333–1349, doi:10.1175/BAMS-D-13-00255.1.

Knutson, T. R., F. Zeng, and A. T. Wittenberg (2013), Multimodel assessment of regional surface temperature trends: CMIP3 and CMIP5 twentieth-century simulations, *J. Clim.*, *26*(22), 8709–8743.

Koster, R. D., et al. (2011), The second phase of the global land–atmosphere coupling experiment: Soil moisture contributions to subseasonal forecast skill, *J. Hydrometeorol.*, *12*(5), 805–822, doi:10.1175/2011JHM1365.1.

Kumar, S., V. Merwade, J. L. Kinter, and D. Niyogi (2013a), Evaluation of temperature and precipitation trends and long-term persistence in CMIP5 twentieth-century climate simulations, *J. Clim.*, *26*(12), 4168–4185.

Kumar, S., J. Kinter, P. A. Dirmeyer, Z. Pan, and J. Adams (2013b), Multidecadal climate variability and the "Warming Hole" in North America: Results from CMIP5 twentieth- and twenty-first-century climate simulations, *J. Clim.*, *26*(11), 3511–3527.

Kumar, S., P. A. Dirmeyer, V. Merwade, T. DelSole, J. M. Adams, and D. Niyogi (2013c), Land use/cover change impacts in CMIP5 climate simulations: A new methodology and 21st century challenges, *J. Geophys. Res. Atmos.*, *118*, 6337–6353, doi:10.1002/jgrd.50463.

Kumar, S., D. M. Lawrence, P. A. Dirmeyer, and J. Sheffield (2014a), Less reliable water availability in the 21st century climate projections, *Earths Future*, *2*(3), 152–160.

Kumar, S., et al. (2014b), Effects of realistic land surface initializations on subseasonal to seasonal soil moisture and temperature predictability in North America and in changing climate simulated by CCSM4, *J. Geophys. Res. Atmos.*, *119*, 13,250–13,270, doi:10.1002/2014JD022110.

Liu, C., and R. P. Allan (2013), Observed and simulated precipitation responses in wet and dry regions 1850–2100, *Environ. Res. Lett.*, *8*(3), 034002, doi:10.1088/1748-9326/8/3/034002.

Lu, J., G. A. Vecchi, and T. Reichler (2007), Expansion of the Hadley cell under global warming, *Geophys. Res. Lett.*, *34*, L06805, doi:10.1029/2006GL028443.

Meehl, G. A., J. M. Arblaster, and C. T. Y. Chung (2015), Disappearance of the southeast U.S. "warming hole" with the late 1990s transition of the Interdecadal Pacific Oscillation, *Geophys. Res. Lett.*, *42*, 5564–5570, doi:10.1002/2015GL064586.

O'gorman, P. A., R. P. Allan, M. P. Byrne, and M. Previdi (2012), Energetic constraints on precipitation under climate change, *Surv. Geophys.*, *33*(3–4), 585–608.

Pitman, A. J., et al. (2009), Uncertainties in climate responses to past land cover change: First results from the LUCID intercomparison study, *Geophys. Res. Lett.*, *36*, L14814, doi:10.1029/2009GL039076.

Roderick, M. L., F. Sun, W. H. Lim, and G. D. Farquhar (2014), A general framework for understanding the response of the water cycle to global warming over land and ocean, *Hydrol. Earth Syst. Sci.*, *18*(5), 1575–1589.

Roderick, M. L., P. Greve, and G. D. Farquhar (2015), On the assessment of aridity with changes in atmospheric CO_2, *Water Resour. Res.*, *51*, 5450–5463, doi:10.1002/2015WR017031.

Santer, B. D., et al. (2007), Identification of human-induced changes in atmospheric moisture content, *Proc. Natl. Acad. Sci. U.S.A.*, *104*(39), 15,248–15,253.

Scheff, J., and D. Frierson (2012), Twenty-first-century multimodel subtropical precipitation declines are mostly midlatitude shifts, *J. Clim.*, *25*(12), 4330–4347.

Scheff, J., and D. M. W. Frierson (2014), Scaling potential evapotranspiration with greenhouse warming, *J. Clim.*, *27*(4), 1539–1558.

Seager, R., N. Naik, and G. A. Vecchi (2010), Thermodynamic and dynamic mechanisms for large-scale changes in the hydrological cycle in response to global warming*, *J. Clim.*, *23*(17), 4651–4668.

Seager, R., D. Neelin, I. Simpson, H. Liu, N. Henderson, T. Shaw, Y. Kushnir, M. Ting, and B. Cook (2014), Dynamical and thermodynamical causes of large-scale changes in the hydrological cycle over North America in response to global warming*, *J. Clim.*, *27*(20), 7921–7948.

Sheffield, J., E. F. Wood, and M. L. Roderick (2012), Little change in global drought over the past 60 years, *Nature*, *491*(7424), 435−438.

Sheffield, J., et al. (2013), North American climate in CMIP5 experiments. Part I: Evaluation of historical simulations of continental and regional climatology, *J. Clim.*, *26*(23), 9209–9245.

Stull, R. B., and C. D. Ahrens (2000), *Meteorology for Scientists and Engineers*, vol. xvi, p. 502, 2nd ed., Brooks/Cole, Pacific Grove, Calif.

Taylor, C. M., R. A. M. de Jeu, F. Guichard, P. P. Harris, and W. A. Dorigo (2012), Afternoon rain more likely over drier soils, *Nature*, *489*(7416), 423–426.

Taylor, K. E., R. J. Stouffer, and G. A. Meehl (2012), An overview of CMIP5 and the experiment design, *Bull. Am. Meteorol. Soc.*, *93*(4), 485–498.

Tietsche, S., J. J. Day, V. Guemas, W. J. Hurlin, S. P. E. Keeley, D. Matei, R. Msadek, M. Collins, and E. Hawkins (2014), Seasonal to interannual Arctic sea ice predictability in current global climate models, *Geophys. Res. Lett.*, *41*, 1035–1043, doi:10.1002/2013GL058755.

Vecchi, G. A., and B. J. Soden (2007), Global warming and the weakening of the tropical circulation, *Bull. Am. Meteorol. Soc.*, *88*(10), 1529–1530.

Villamayor, J., and E. Mohino (2015), Robust Sahel drought due to the Interdecadal Pacific Oscillation in CMIP5 simulations, *Geophys. Res. Lett.*, *42*, 1214–1222, doi:10.1002/2014GL062473.

Zhang, D., Z. Cong, G. Ni, D. Yang, and S. Hu (2015), Effects of snow ratio on annual runoff within the Budyko framework, *Hydrol. Earth Syst. Sci.*, *19*(4), 1977–1992.

Zhang, L., N. Potter, K. Hickel, Y. Zhang, and Q. Shao (2008), Water balance modeling over variable time scales based on the Budyko framework—Model development and testing, *J. Hydrol.*, *360*(1–4), 117–131.